~~Revealing the~~ Underestimation of Anthropogenic Organosulfates in Atmospheric Aerosols in Urban Regions

Yanting Qiu[1#], Junrui Wang[1#], Tao Qiu[2], Jiajie Li[3], Yanxin Bai[4], Teng Liu[1], Ruiqi Man[1], Taomou Zong[1], Wenxu Fang[1], Jiawei Yang[1], Yu Xie[1], Zeyu Feng[1], Chenhui Li[3], Ying Wei[3], Kai Bi[5], Dapeng Liang[2], Ziqi Gao[6], Zhijun Wu[1,], Yuchen Wang[4,*], Min Hu[1]*

[1] State Key Laboratory of Regional Environment and Sustainability, College of Environmental Sciences and Engineering, Peking University, Beijing 100871, China;

[2] Key Lab of Groundwater Resources and Environment of the Ministry of Education, College of New Energy and Environment, Jilin University, Changchun 130012, China

[3] College of Environment and Ecology, Laboratory of Compound Air Pollutions Identification and Control, Taiyuan University of Technology, Taiyuan, 030024, China

[4] College of Environmental Science and Engineering, Hunan University, Changsha, Hunan, 410082, China

[5] Beijing Weather Modification Center, Beijing Meteorological Service, Beijing, China

[6] University of Virginia Environmental Institute, Charlottesville, VA 22902, United States

#: Yanting Qiu and Junrui Wang contributed equally to this work

*Correspondence Author:

Zhijun Wu (zhijunwu@pku.edu.cn) and Yuchen Wang (ywang@hnu.edu.cn)

ABSTRACT

Organosulfates (OSs) are important components of organic aerosols, which serve as critical tracers of secondary organic aerosols (SOA). However, molecular composition, ~~classification~~precursor-OS correspondence, and formation driving factors of OSs at different atmospheric conditions have not been fully constrained. In this work, we integrated OS~~s~~ molecular composition, precursor-constrained positive matrix factorization (PMF) source apportionment, and OS~~s~~-precursor correlation analysis to classify OS~~s~~ detected from $PM_{2.5}$ samples according to their volatile organic compounds (VOCs) precursors collected from three different cities (Beijing, Taiyuan, and Changsha) in China. This new approach enables the accurate classification of OSs from molecular perspective. Compared with conventional classification methods, we found the mass fraction of Aliphatic OSs ~~and~~ (including nitrooxy OSs ~~(~~; NOSs) increased by 22.0%, 17.8%, and 10.3% in Beijing, Taiyuan, and Changsha, respectively, highlighting the underestimation of Aliphatic OSs ~~and NOSs~~ in urban regions. The formation driving factors of Aliphatic OSs ~~and NOSs~~ were further investigated. We found that elevated aerosol liquid water content promoted the formation of Aliphatic OSs ~~and NOSs~~ only when aerosols transition from non-liquid state to liquid state. In addition, enhanced inorganic sulfate mass concentrations, and O_x ($O_x = NO_2 + O_3$) concentrations, as well as decreased aerosol pH commonly facilitated the formation of Aliphatic OSs ~~and NOSs~~. These results reveal a significant underestimation of OSs derived from anthropogenic emissions, particularly Aliphatic OSs, highlighting the need for a deeper understanding of SOA formation and composition in urban environments.~~These results reveal the underestimation of OS derived from anthropogenic emission, highlighting the potential indicative role of Aliphatic OSs and NOSs in urban SOA.~~

KEY WORDS: organosulfate; non-target analysis; high-resolution mass spectrometry; secondary organic aerosol; PMF source apportionment

1. Introduction

Due to the diversity of natural and anthropogenic emissions and the complexity of atmospheric chemistry, investigating the chemical characterization and formation mechanisms of secondary organic aerosols (SOA) remains challenging. Among SOA components, organosulfates (OSs) have emerged as key tracers (Brüggemann et al., 2020; Hoyle et al., 2011), as their formation is primarily governed by secondary atmospheric processes. Moreover, OS~~s~~ significantly influence the aerosol physicochemical properties, including acidity (Riva et al., 2019; Zhang et al., 2019), hygroscopicity (Estillore et al., 2016; Ohno et al., 2022; Hansen et al., 2015), and light-absorption properties (Fleming et al., 2019; Jiang et al., 2025). Therefore, a deeper understanding of OS~~s~~ abundance, sources, and formation drivers is crucial for elucidating SOA formation and its properties.

Quantifying OS~~s~~ abundance is ~~vital~~ critical to assess their contribution to SOA. However, this is difficult due to the large number and structural diversity of OSs molecules and the lack of authentic standards. Most studies quantify a few representative OSs using synthetic or surrogate standards (Wang et al., 2020; Wang et al., 2017; Huang et al., 2018b; He et al., 2022), while non-target analysis (NTA) with high-resolution mass spectrometry (HRMS) offers broader molecular characterization (Huang et al., 2023a; Wang et al., 2022b; Cai et al., 2020). Although NTA combined with surrogate standards allows molecular-level (semi-)quantification, overall OS mass concentration~~s~~ remain underestimated, and many OS~~s~~s remain unidentified (Lukács et al., 2009; Cao et al., 2017; Tolocka and Turpin, 2012; Ma et al., 2025).

C~~Accurate classification of~~lassifying OS~~s~~ ~~by~~ based on their precursors is ~~essential for reliable quantification and mechanistic insights~~a powerful approach for understanding OS formation from a mechanistic perspective. OSs from specific precursors generally share similar elemental compositions, with characteristic ranges of C atoms, double bond equivalents (DBE), and aromaticity equivalents (Xc). For example, isoprene-derived OSs typically contain 4–5 C atoms; monoterpene- and sesquiterpene-derived OSs usually have 9–10 and 14–15 C atoms, respectively (Lin et al., 2012; Riva et al., 2016c; Wang et al., 2019a; Surratt et al., 2008; Riva et al., 2015). An "OS precursor map," correlating molecular weight and carbon number based on chamber studies, has been developed to classify OSs accordingly (Wang et al., 2019a). However, these approaches often oversimplify OS~~s~~ formation by relying solely on elemental composition, leaving many OSs without identified precursors.

The formation mechanisms of OS~~s~~ remain incompletely understood, though several driving factors have been identified through controlled chamber experiments and ambient observations. For instance, increased aerosol liquid water content (ALWC) enhances OS~~s~~ formation by promoting the uptake of gaseous precursors (Xu et al., 2021a; Wang et al., 2021b) ~~(Edwards et al., 2017; Brown et al., 2012)~~. Inorganic sulfate can also affect OS~~s~~ formation by acting as nucleophiles via epoxide pathway (Eddingsaas et al., 2010; Wang et al., 2020). However, meteorological conditions vary across cities, meaning the relative importance of these factors may differ by location. Thus, evaluating these formation drivers under diverse atmospheric conditions is essential. Identifying both common and region-specific drivers is key to a comprehensive understanding of OS~~s~~ formation mechanisms.

In this study, we employed ~~non-target analysis (~~NTA~~)~~ using ultra-high performance liquid chromatography (UHPLC) coupled with high-resolution mass spectrometry (HRMS) to characterize

OS~~s~~ molecular composition in $PM_{2.5}$ samples from three cities. Identified OSs were classified by their VOCs precursors~~—~~, including aromatic, aliphatic, monoterpene, and sesquiterpene VOCs~~—~~, via precursor-constrained positive matrix factorization (PMF). Mass concentrations were quantified or semi-quantified using authentic or surrogate standards. Additionally, spatial variations in OS concentrations and co-located environmental factors were analyzed to distinguish both common and site-specific drivers of OS formation.

2. Methodology

2.1 Sampling and Filter Extraction

Field observations were conducted during winter (December 2023 to January 2024) at three urban sites in China: Beijing, Taiyuan, and Changsha. The site selection was based on contrasts in winter meteorological conditions and dominate $PM_{2.5}$ sources. For meteorological conditions, Beijing and Taiyuan represent northern Chinese cities with cold, dry conditions (low RH). In comparison, Changsha is characterized by relatively higher winter RH. In terms of $PM_{2.5}$ sources, Taiyuan is a traditional industrial and coal-mining base, Changsha's pollution profile is more influenced by traffic and domestic cooking emissions, whereas Beijing is characterized by a high mass fraction of secondary aerosols. This enables a comparative analysis of OS formation mechanisms under varied atmospheric conditions. In Beijing, $PM_{2.5}$ samples were collected at the Peking University Atmosphere Environment Monitoring Station (PKUERS; 40.00°N, 116.32°E), as detailed in previous studies (Wang et al., 2023a). Sampling in Taiyuan and Changsha took place on rooftops at the Taoyuan National Control Station for Ambient Air Quality (37.88°N, 112.55°E) and the Hunan Hybrid Rice Research Center (28.20°N, 113.09°E), respectively (see Figure S1).

Daily $PM_{2.5}$ samples were collected on quartz fiber filters (φ = 47 mm, Whatman Inc.) from 9:00 to 8:00 local time the next day. All quartz fiber filters were pre-baked at 550 °C before sampling to remove the background organic matters. In Beijing and Taiyuan, RH-resolved sampling was performed using an RH-resolved sampler, stratifying daily samples into low (RH ≤ 40%), moderate (40% < RH ≤ 60%), and high (RH > 60%) RH regimes with the sampling flow rate of 38 L/min. Due to persistently high RH in Changsha, a four-channel sampler (TH-16, Wuhan Tianhong Inc.) collected $PM_{2.5}$ samples without RH stratification with the flow rate of 16.7 L/min. Consequently, Beijing and Taiyuan collected one or more samples daily, whereas Changsha collected one sample per day. A total of 40, 64, and 30 samples were obtained from Beijing, Taiyuan, and Changsha, respectively. The samples were stored in a freezer at -18 °C immediately after collection. The maximum duration between the completion of sampling and the start of chemical analysis was approximately 40 days. Prior to analysis, all samples were equilibrated for 24 hours under controlled temperature (20 ± 1 °C) and RH (40-45%) within a clean bench, in order to allow the filters to reach a stable, reproducible condition for subsequent handling and to minimize moisture condensation. Average daily $PM_{2.5}$ mass concentrations and RH during sampling are summarized in Table S1.

Sample extraction followed established protocols (Wang et al., 2020). Briefly, filters were ultrasonically ~~–~~extracted twice for 20 minutes. A total volume of 10 mL ~~with~~of LC-MS grade methanol (Merck Inc.) was used for each sample~~,~~. All extracts were filtered through 0.22 μm PTFE

syringe filters, and evaporated under a gentle stream of high-purity N_2 (>99.99%). The dried extracts were then redissolved in 2 mL of LC-MS grade methanol for analysis. This step was necessary to achieve sufficient sensitivity for the detection of OSs with low concentration.

During the campaign, gaseous pollutants (SO_2, NO_2, O_3, CO) were monitored using automatic analyzers. $PM_{2.5}$ and PM_{10} mass concentrations were measured by tapered element oscillating microbalance (TEOM). Water-soluble ions (Na^+, NH_4^+, K^+, Mg^{2+}, Ca^{2+}, Cl^-, NO_3^-, SO_4^{2-}) were analyzed with the Monitor for AeRosols and Gases in ambient Air (MARGA) coupled with ion chromatography. Organic carbon (OC) and elemental carbon (EC) were quantified by online OC/EC analyzers or carbon aerosol speciation systems. Trace elements in $PM_{2.5}$ were determined by X-ray fluorescence spectrometry (XRF). Additionally, VOCs concentrations were measured using an online gas chromatography-mass spectrometry (GC-MS) system with a one-hour time resolution in Taiyuan and Changsha. Table S2 summarizes the monitoring instruments deployed at each site. All instruments were calibrated to ensure the reliability of the measurement data. Specifically, the online gas pollutants and particulate matter automatic analyzers underwent automatic zero/span checks every 24 hours at 0:00 local time. For MARGA-ion chromatography, OC/EC analyzers, and XRF systems were calibrated weekly. The online GC-MS system was automatically calibrated every 24 hours using standard VOCs mixture.

2.2 Identification of Organosulfates

The molecular composition of $PM_{2.5}$ extracts was analyzed using an ultra-high performance liquid chromatography (UHPLC) system (Thermo Ultimate 3000, Thermo Scientific) coupled with an Orbitrap HRMS (Orbitrap Fusion, Thermo Scientific) equipped with an electrospray ionization (ESI) source operating in negative mode. Chromatographic separation was achieved on a reversed-phase Accucore C18 column (150 × 2.1 mm, 2.6 μm particle size, Thermo Scientific). For tandem MS acquisition, full MS scans (*m/z* 70–700) were collected at a resolving power of 120,000, followed by data-dependent MS/MS (ddMS^2) scans (*m/z* 50–500) at 30,000 resolving power. Detailed UHPLC-HRMS^2 parameters are provided in Text S1.

NTA was performed using Compound Discoverer (CD) software (version 3.3, Thermo Scientific) to identify chromatographic peak features (workflow details in Table S3). Molecular formulas were assigned based on elemental combinations $C_cH_hO_oN_nS_s$ (c = 1–90, h = 1–200, o = 0–20, n = 0–1, s = 0–1) within a mass tolerance of 0.005 Da with up to one ^{13}C isotope. Formulas with hydrogen-to-carbon (H/C) ratios outside 0.3–3.0 and oxygen-to-carbon (O/C) ratios beyond 0–3.0 were excluded to remove implausible assignments. We calculated the double bond equivalent (DBE) and aromatic index represented by Xc based on assigned elemental combinations using eqs. (1) and (2), where *m* and *k* were the fractions of oxygen and sulfur atoms in the π-bond structures of a compound (both *m* and *k* were presumed to be 0.50 in this work (Yassine et al., 2014)). ~~Double bound equivalent (DBE) and Xc (Ma et al., 2022) were calculated using eqs. (1) and (2), where *m* and *k* were the fractions of oxygen and sulfur atoms in the π-bond structures of a compound (both *m* and *k* were presumed to be 0.50 in this work (Yassine et al., 2014)).~~

$$DBE = c - 0.5h + 0.5n + 1 \quad (1)$$

$$Xc = \begin{cases} (3 \times (DBE - m \times o - k \times s) - 2)/(DBE - m \times o - k \times s) & (if\ \ DBE < (m \times o + \end{cases}$$

$k \times s)$ or $Xc < 0$, $then$ Xc was set to $0)$ (2)

In eq. (2), Xc is an important indicator of whether aromatic rings exist in a molecule. Studies have proved that a molecule is considered aromatic if its Xc value exceeds 2.50 (Ma et al., 2022; Yassine et al., 2014). OSs were selected based on compounds with O/S ≥ 4 and HSO_4^- (*m/z* 96.96010) ~~and/or SO_3^- (*m/z* 79.95736)~~ fragments were observed in their corresponding MS^2 spectra. Among them, if N number is 1, O/S ≥ 7, and their MS^2 spectra showed ONO_2^- (*m/z* 61.98837) fragment, these OSs were defined as nitrooxy OSs (NOSs). It should be noted that several CHOS (composed of C, H, O, and S atoms, hereinafter) and CHONS species were not determined as OSs due to their low-abundance and insufficient to trigger reliable data-dependent MS^2 acquisition, which may lead to an underestimation of total OS mass concentration.

2.3 Classification and Quantification/Semi-quantification of Organosulfates

To ensure the reliability of quantitative analysis and source attribution, this study focuses on OS species with C ≥ 8. The exclusion of smaller OSs (C ≤ 7) is based on challenges in their unambiguous identification, including co-elution with interfering compounds (Liu et al., 2024), and higher uncertainty in precursor assignment due to the lack of characteristic "tracer" molecules in laboratory experiments. Though redisslove using pure methanol may not be the ideal solvent for retaining polar, early-eluting compounds on the reversed-phase column, it provided a consistent solvent for the analysis of the mid- and non-polar OS species (C ≥ 8) that are the focus of this study.

~~Due to reversed-phase column limitations, concentration estimates of small OSs (C ≤ 7) are highly uncertain (Liu et al., 2024); thus, only OSs with C ≥ 8 were analyzed.~~ To classify the identified OSs, we employed and compared two distinct classification approaches. Firstly, a conventional classification approach relies primarily on precursor–product relationships established through controlled laboratory chamber experiments and field campaigns ~~Firstly, we used conventional classification approach following previous studies~~ (Zhao et al., 2018; Wang et al., 2021a; Deng et al., 2021; Xu et al., 2021b; Mutzel et al., 2015; Brüggemann et al., 2020; Yang et al., 2024; Duporté et al., 2020; Huang et al., 2023b; Wang et al., 2022b; Riva et al., 2016a). Based on these established precursor–product relationships, ~~All~~ detected OSs and NOSs were classified into ~~seven~~ four groups: Monoterpene OSs ~~and~~ (including Monoterpene NOSs, hereinafter), Aliphatic OSs (including Aliphatic NOSs, hereinafter), Aromatic OSs ~~and~~ (including Aromatic NOSs, hereinafter), and Sesquiterpene OSs ~~and~~ (including Sesquiterpene NOSs, hereinafter) (see Table S4 for details). ~~NOSs from aliphatic precursors were not observed. Those without identified precursors were labeled Unknown OSs or NOSs.~~ It is apparently that this approach has notable limitations when applied to detected OS in atmospheric aerosols. A substantial fraction of detected OSs does not match known laboratory tracers and are thus labeled Unknown OSs (including Unknown NOSs, hereinafter).

Synthetic α-pinene OSs ($C_{10}H_{17}O_5S^-$) and NOSs ($C_{10}H_{16}NO_7S^-$) served for (semi-)quantifying Monoterpene and Sesquiterpene OSs ~~and NOSs~~. Their detailed synthesis procedure was described in previous study (Wang et al., 2019b). Potassium phenyl sulfate ($C_6H_5O_4S^-$) and sodium octyl sulfate ($C_8H_{17}O_4S^-$) were used for Aromatic OSs ~~and NOSs~~ and Aliphatic OSs due to lack of authentic standards (Yang et al., 2023; He et al., 2022; Staudt et al., 2014). Unknown OSs ~~and NOSs~~ were semi-quantified by surrogates with similar retention times (RT) (Yang et al., 2023; Huang et al., 2023b). Table 1 lists the standards, retention times, and quantified categories. Unknown OSs ~~and NOSs~~ were

absent between 2.00–5.00 min and after 13.60 min.

Table 1 Chemical structure, UHPLC retention time, and quantified categories of standards used in the quantification/semi-quantificaiton of OSs and NOSs

Formula (M-H)	*m/z* ([M-H]$^-$)	Chemical structure	UHPLC RT (min)	Quantified OSs categories
$C_6H_5O_4S^-$	172.99140	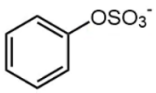	0.92	Aromatic OSs ~~and NOSs~~, Unknown OSs ~~and NOSs~~ (RT 0.50-2.00 min)
$C_8H_{17}O_4S^-$	209.08530	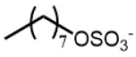	10.30	Aliphatic OSs, Unknown OSs ~~and NOSs~~ (RT 10.00-13.60 min)
$C_{10}H_{17}O_5S^-$	249.08022	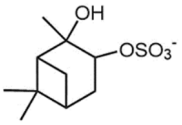	7.73	Monoterpene OSs, Sesquiterpene OSs, Unknown OSs ~~and NOSs~~ (RT 5.00-10.00 min)
$C_{10}H_{16}NO_7S^-$	294.06530		9.26	Monoterpene NOSs and Sesquiterpene NOSs

This quantification approach introduces inherent uncertainty, as differences in molecular structure and functional groups between a surrogate and detected OSs have different ionization efficiency (Ma et al., 2025), which is a well-documented challenge in NTA of complex mixtures. However, this approach provides a consistent basis for comparing the relative abundance of OS in different cities and their formation driving factors. Hence, the mass concentration of detected OSs is still reliable in understanding their classification and formation driving factors.

To classify the Unknown OSs ~~and NOSs~~, we first calculated the Xc of each specie. Those with DBE > 2 and Xc > 2.50 were designated as Aromatic OSs ~~and NOSs~~ (Yassine et al., 2014). Subsequently, constrained positive matrix factorization (PMF) analysis was performed using EPA PMF 5.0~~.~~. The input matrix comprised the mass concentrations of 60 unclassified OS species across all samples.

Figure S2 shows the source profiles of PMF model. Four factors were identified in this study. Specifically, Factor 1 is identified as Aliphatic OSs due to the dominant contributions from species like $C_{11}H_{22}O_5S$ and $C_{12}H_{24}O_5S$, which possess low DBE and are characteristic of long-chain alkane oxidation (Yang et al., 2024). This assignment is strongly supported by the co-variation of this factor with n-dodecane. Similarly, Factor 2 is classified as Aromatic OSs, highlighted by the significant contribution of $C_{10}H_{10}O_7S$ and $C_{11}H_{14}O_7S$, which have been proved as OSs derived from typical aromatic VOCs (Riva et al., 2015). In addition, the high contributions of benzene, toluene, and styrene in Factor 2 further suggests that this factor should be classified as Aromatic OSs. As for Factor 3 and Factor 4 is confirmed by the prominence of established Monoterpene OSs (Surratt et al., 2008; Iinuma et al., 2007) (e.g., $C_{10}H_{18}O_5S$, $C_{10}H_{17}NO_7S$) and Sesquiterpene OSs (Wang et al., 2022b) (e.g., $C_{14}H_{28}O_6S$, $C_{15}H_{25}NO_7S$), respectively. Moreover, isoprene showed high contribution in both Factors

3 and 4. As monoterpenes and sesquiterpenes cannot be detected by online GC-MS, considering that monoterpenes and sesquiterpenes mainly originate from biogenic sources and ~~Given monoterpenes and sesquiterpenes primarily originate from biogenic sources and strongly correlate with isoprene ;~~strongly correlate with isoprene (Guenther et al., 2006; Sakulyanontvittaya et al., 2008), therefore, isoprene is used as a surrogate marker as Monoterpene OSs and Sesquiterpene OSs. High contribution of isoprene in Factors 3 and 4 proved that these factors were respectively determined as Monoterpene OSs and Sesquiterpene OSs. ~~Several OSs with known precursors served as auxiliary tracers to guide source apportionment. Specifically, $C_{11}H_{22}O_5S$ and $C_{12}H_{24}O_5S$ for long-chain aliphatic OSs (Yang et al., 2024); $C_{10}H_{10}O_7S$ and $C_{11}H_{14}O_7S$ for Aromatic OSs and NOSs (Riva et al., 2015); $C_{10}H_{18}O_5S$ and $C_{10}H_{17}NO_7S$ for Monoterpene OSs and NOSs, respectively (Surratt et al., 2008; Iinuma et al., 2007); $C_{14}H_{28}O_6S$ and $C_{15}H_{25}NO_7S$ for Sesquiterpene OSs and NOSs, respectively (Wang et al., 2022b). These were selected due to their high detection frequency (>85%) and the highest average concentrations within their categories. Typical VOCs markers (isoprene, benzene, toluene, styrene, n-dodecane) were also included in the PMF model.~~ Based on marker species, Unknown OSs ~~and NOSs~~ were further categorized into ~~eight groups:~~ Monoterpene, Aromatic, Aliphatic, and Sesquiterpene OSs ~~and NOSs~~.

The model was executed with 10 runs to ensure stability. The ratio of Q_{robust}/Q_{true} for this solution was stabilized below 1.50, indicating a robust fit without over-factorization. Furthermore, the scaled residual matrix (see Figure S3), demonstrating that residuals are randomly distributed and predominantly within the acceptable range of -3 to 3. Correlation coefficients between classified OSs~~/NOSs~~ and corresponding VOCs (Monoterpene OSs ~~and NOSs~~ vs. isoprene; Aromatic OSs ~~and NOSs~~ vs. benzene; Aliphatic OSs ~~and NOSs~~ vs. n-dodecane; Sesquiterpene OSs ~~and NOSs~~ vs. isoprene) were calculated as a statistical auxiliary variable to verify the reliability of PMF results~~,~~. The arithmetic mean of hourly VOCs within each corresponding filter sampling period was calculated to align the time resolution of VOCs and OS mass concentration. ~~excluding s~~Species with $R < 0.40$ were excluded to avoid potential incorrect classification. ~~Given monoterpenes and sesquiterpenes primarily originate from biogenic sources and strongly correlate with isoprene. Therefore, we checked the relationship between Monoterpene OSs and NOSs, Sesquiterpene OSs and NOSs, and isoprene.~~

To validate classification accuracy, MS^2 fragment patterns were analyzed (Table S5). Diagnostic fragments supported the assignments: Aliphatic OSs ~~and NOSs~~ showed sequential alkyl chain cleavages (Δ m/z = 14.0157) and saturated alkyl fragments ($[C_nH_{2n+1}]^-$ or $[C_nH_{2n-1}]^-$); Monoterpene OSs ~~and NOSs~~ displayed $[C_nH_{2n-3}]^-$ fragments; Aromatic OSs~~/NOSs~~ exhibited characteristic aromatic substituent fragments ($[C_6H_5R\text{-}H]^-$, R = alkyl, carbonyl, -OH, or H). While absolute certainty for every individual OS in a complex ambient mixture is unattainable, integrating the precursor-constrained PMF model, tracer VOCs correlation analysis, and MS^2 fragment patterns validation significantly reduces the likelihood of systematic misclassification.~~These fragment patterns confirm the reliability of our classification approach.~~

3. Results and Discussion

3.1 Concentrations, Compositions, and Classification of Organosulfates

Figure 1 shows the temporal variations of OS and organic aerosols (OA) mass concentrations, as well as RH, during the sampling period across the three cities. The total mass concentration of OS reported in this study is the sum of the (semi-)quantified concentrations of all individual OS species that met the identification criteria described in Section 2.3. The mean OSs concentrations were (41.1~~1~~ ± 34.4~~7~~5) ng/m^3 in Beijing, (57.~~39~~ 4 ± 39.2~~3~~) ng/m^3 in Taiyuan, and (102.~~06~~ 1 ± 80.5~~4~~) ng/m^3 in Changsha. Table S6 summarizes the average concentrations of $PM_{2.5}$, OC, gaseous pollutants, OS mass concentrations, and the mean meteorological parameters during sampling period for all three cities. OS accounted for 0.64% ± 0.44%, 0.41% ± 0.24%, and 0.76% ± 0.34% of the total OA in Beijing, Taiyuan, and Changsha, respectively.

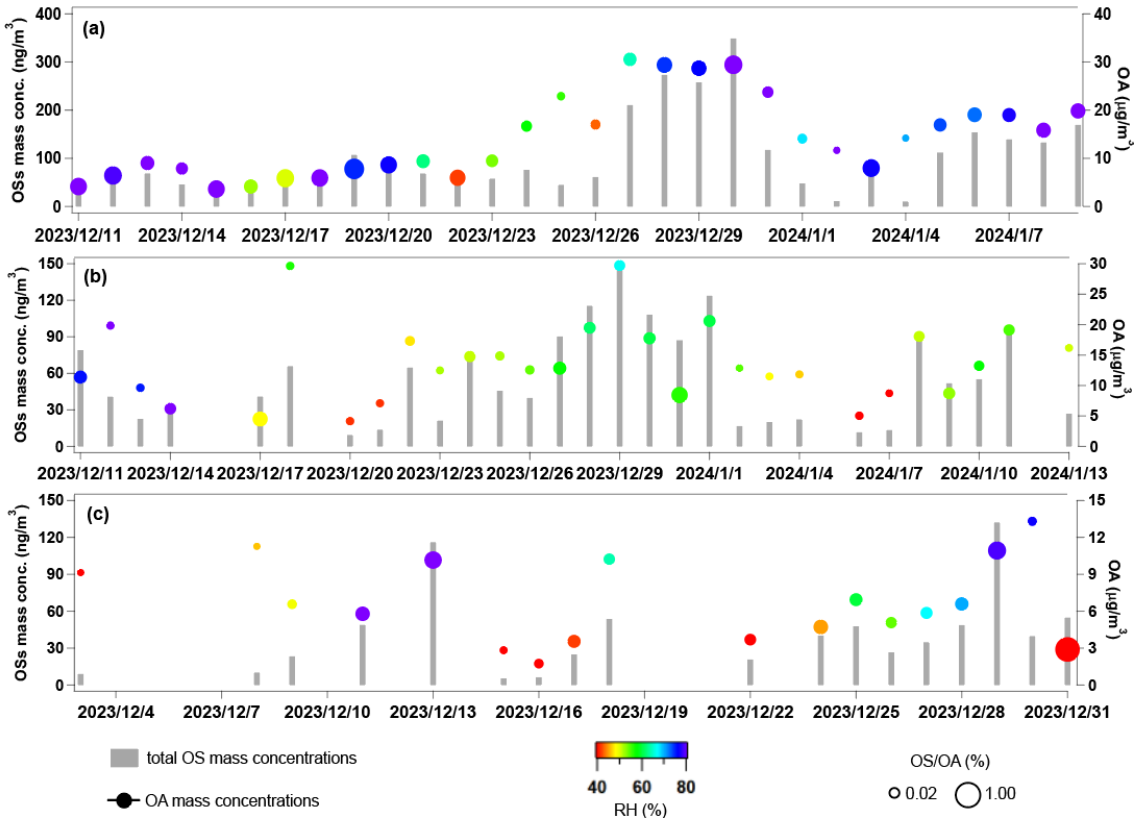

Figure 1 Temporal variations of daily total OS mass concentrations and average OA mass concentrations in (a) Changsha, (b) Taiyuan, and (c) Beijing. The markers of OA mass concentrations are colored by average RH during sampling period, and marker sizes indicate the OS/OA mass concentration ratios.

The highest OS mass concentrations and OS/OA ratios were observed in Changsha. As shown in Figure 1(a), a distinct episode with OS mass concentrations exceeding 300 ng/m^3 occurred between December 27th and 31st, leading to the elevated OS mass concentrations in Changsha. This episode coincided with a period of intense fireworks activity, as evidenced by significant increases in the concentrations of recognized fireworks tracers, especially Ba and K (see Figure S4), leading to an

increase in SO_2 emission. We noted that though K may originate from biomass burning, its trend in concentration shows good consistency with that of Ba. Therefore, we still infer that fireworks activity are also the primary source of K. Considering persistently high RH (consistently >70%) during this period, as displayed in Figure S5, ALWC (117.9 μg/m^3 in average) therefore increased and facilitated the heterogeneous oxidation of SO_2 to particulate sulfate (Wang et al., 2016a; Ye et al., 2023). Since particulate sulfate serves as a key reactant in OS formation pathways, its elevated concentration directly promoted OS production (Xu et al., 2024; Wang et al., 2020). Furthermore, fireworks activity led to concurrent increases in the concentrations of transition metals, notably Fe and Mn (Figure S4), which are known to catalyze aqueous-phase radical chemistry and OS formation (Huang et al., 2019; Huang et al., 2018a). Therefore, the pronounced OS mass concentration during this period is attributed to a combination of elevated precursor emissions (SO_2), high-RH conditions favoring aqueous-phase processing, and the potential catalytic role of co-emitted transition metals.

It is noteworthy that the single highest OS/OA ratio in Beijing was observed on December 31st under low RH. This phenomena highlights that ALWC, while a major driving factor of OS formation, is not an exclusive control. Specifically, this day showed high atmospheric oxidative capacity and aerosol acidity. We note that under such conditions, efficient acid-catalyzed heterogeneous reactions of gas-phase oxidation products could drive substantial OS formation. The impact of ALWC, atmospheric oxidative capacity, and aerosol pH on OS formation will be discussed in detail in Section 3.2.

~~During this period, RH remained consistently above 70%, and the resulting increase in ALWC facilitated OSs formation through aqueous-phase reactions~~ (Cheng et al., 2016a; Wu et al., 2018; Zheng et al., 2015)~~. Furthermore, as shown in Figure S4, concentrations of Ba and K, tracers for fireworks emissions, were elevated, indicating intense fireworks activity. The high ALWC accelerated the heterogeneous conversion of SO_2 from fireworks into particulate sulfate (Figure S5), further promoting OSs formation (Xu et al., 2024; Wang et al., 2020). Additionally, transition metals such as Fe and Mn, emitted during fireworks combustion (Figure S4), catalyzed OS formation (Huang et al., 2019; Huang et al., 2018a). Collectively, these factors contributed to the pronounced OS mass concentration observed during this period.~~

Figures 2(a) and 2(b) shows the average mass concentrations and fractions of different OSs categories across the three cities, based on classification approach based on OSs' elemental composition and laboratory chamber-derived precursor–OS relationships~~conventional~~ and our precursor-based PMF classification approach developed in this work~~new classification approach~~, respectively (see Section 2.3 for details). As displayed in Figure 2(b), Monoterpene OSs ~~and NOSs~~ dominated detected OSs across all cities, contributing 55.2% (Beijing), 46.8% (Taiyuan), and 72.3% (Changsha) to total OS, respectively. Biogenic-emitted monoterpene is the precursor of Monoterpene OSs~~ and NOSs~~. However, monoterpenes are primarily biogenic precursors, their limited emissions during winter cannot fully explain the high mass fractions of Monoterpene OSs~~ and NOSs~~. Recent studies have highlighted anthropogenic sources, particularly biomass burning, as significant contributors to monoterpene (Wang et al., 2022a; Koss et al., 2018). The $PM_{2.5}$ source apportionment analysis (Text S2, Figure S6) confirmed that biomass burning substantially contributed to $PM_{2.5}$ across all cities. The highest total mass fractions of Monoterpene OSs ~~and NOSs~~ in Changsha are mainly attributed to the high RH (Table S6), which facilitates their formation via heterogeneous reactions

(Hettiyadura et al., 2017; Wang et al., 2018; Ding et al., 2016a; Ding et al., 2016b; Li et al., 2020).

In Taiyuan, the total mass fractions of Aromatic OSs ~~and NOSs~~ (21.2%) were significantly higher than those in Beijing (10.7%) and Changsha (4.6%). Aromatic OSs ~~and NOSs~~ primarily formed via aqueous-phase reactions between S(IV) and aromatic VOCs (Huang et al., 2020). Taiyuan exhibited the highest sulfate mass concentration among the three cities (Table S6), which promoted the formation of these species. Additionally, transition metal ions—particularly Fe^{3+}—catalyze aqueous-phase formation of Aromatic OSs ~~and NOSs~~ (Huang et al., 2020). High Fe mass concentration was observed in Taiyuan (0.79 ± 0.53 μg/m^3), further facilitated the formation of Aromatic OSs ~~and NOSs.~~.

The highest total mass fractions of Aliphatic OSs ~~and NOSs~~ ~~was~~ were observed in Beijing (28.1%). Since vehicle emissions, which is an important source of long-chain alkenes (He et al., 2022; Wang et al., 2021a; Riva et al., 2016b; Tao et al., 2014; Tang et al., 2020), substantially contributed to $PM_{2.5}$ in all cities (Figure S6), the relative dominance of Aliphatic OSs in Beijing can be attributed to a comparative reduction in the emissions of precursors for Monoterpene OSs and Aromatic OSs. Specifically, Beijing exhibits lower emissions of monoterpene and aromatic VOCs precursors relative to Taiyuan and Changsha, which results in a reduced contribution of Monoterpene and Aromatic OSs to the total OS (see Figure 2(b)). Therefore, the relative mass fraction of Aliphatic OSs, which primarily derived from between sulfate and photooxidation products of alkenes (Riva et al., 2016b), becomes more prominent in Beijing. Additionally, low RH in Beijing further suppresses the aqueous-phase formation of Monoterpene OSs, amplifying the relative importance of Aliphatic OSs. ~~The formation mechanisms of Aliphatic OSs and NOSs still remains highly uncertainty up to now. Potential pathways include heterogeneous reactions between SO_2 and alkenes (Passananti et al., 2016), as well as reactions between sulfate and photooxidation products of alkenes~~ (Riva et al., 2016b)~~. Their precursors, mainly long-chain alkenes, are predominantly emitted from fossil fuel combustion and vehicle emissions~~ (He et al., 2022; Wang et al., 2021a; Riva et al., 2016b; Tao et al., 2014; Tang et al., 2020)~~. Since fossil fuel combustion and vehicle emissions substantially contributed to $PM_{2.5}$ in all cities (Figure S4), it is suggested that relatively low anthropogenic emissions and low RH promote the dominance of Aliphatic OSs and NOSs. Specifically, low anthropogenic emissions reduce the precursor concentrations for Monoterpene OSs/NOSs and Aromatic OSs/NOSs, while low RH limits their formation through aqueous-phase reactions.~~

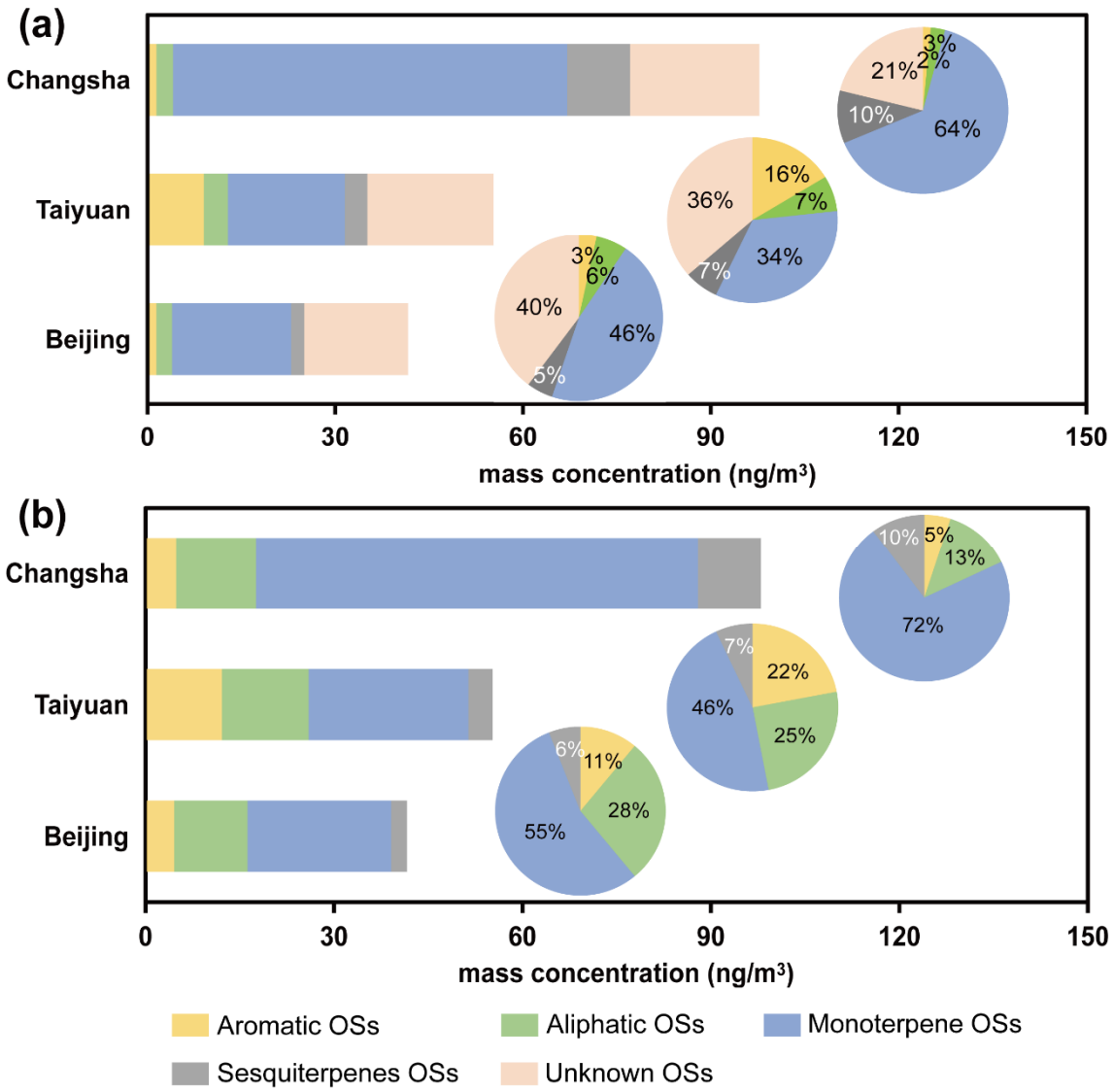

Figure 2 The average mass concentrations of different OSs categories ~~(a) before and (b) after classification across three cities~~using (a) conventional classification approach based on OSs' elemental composition and laboratory chamber-derived precursor–OS relationships and (b) precursor-based PMF classification approach developed in this work across all cities.~~.~~ The inserted pie chart indicates the average mass fractions of different OSs categories.

3.2 Formation Driving Factors of Aliphatic OSs and NOSs

Compared with conventional classification approach (Figure ~~1~~2(a)), we found Aliphatic OSs ~~and NOSs~~ increased markedly~~—~~ (by 22.0%, 17.8%, and 10.3% in Beijing, Taiyuan, and Changsha, respectively~~—~~)~~with Aliphatic NOSs newly identified~~. Therefore, we further examined the formation drivers of Aliphatic OSs ~~and NOSs~~.

ALWC plays a key role in facilitate OSs formation (Wang et al., 2020). Using $PM_{2.5}$ chemical composition and RH, ALWC was calculated via the ISORROPIA-II model (details in Text S3) (Fountoukis and Nenes, 2007). Given the direct influence of ambient RH on ALWC (Figure S7) (Bateman et al., 2014) and leveraging RH-resolved samples from Beijing and Taiyuan, we assessed

RH effects on Aliphatic OSs~~/NOSs~~ under low (RH < 40%), medium (40% ≤ RH < 60%), and high (RH ≥ 60%) conditions.

In Changsha, where RH remains consistently high, Aliphatic OSs ~~and NOSs~~ mass concentrations strongly correlated with RH (R = 0.78). In Beijing and Taiyuan, correlations increased from low to medium RH (Beijing: 0.53 to 0.82; Taiyuan: 0.38 to 0.77) but declined slightly at higher RH (Beijing: 0.82 to 0.69; Taiyuan: 0.77 to 0.72). The initial correlation rise reflects ALWC-enhanced sulfate-driven heterogeneous OS~~s~~ formation (Wang et al., 2016b; Cheng et al., 2016b), while the decline at elevated RH ~~is unexplained.~~may due to the increase in ALWC dilutes the concentrations of precursors and intermediates of Aliphatic OSs within the aqueous phase. Therefore, Aliphatic OSs formation were not further promoted, exhibiting the non-linear response of their mass concentrations and ALWC.

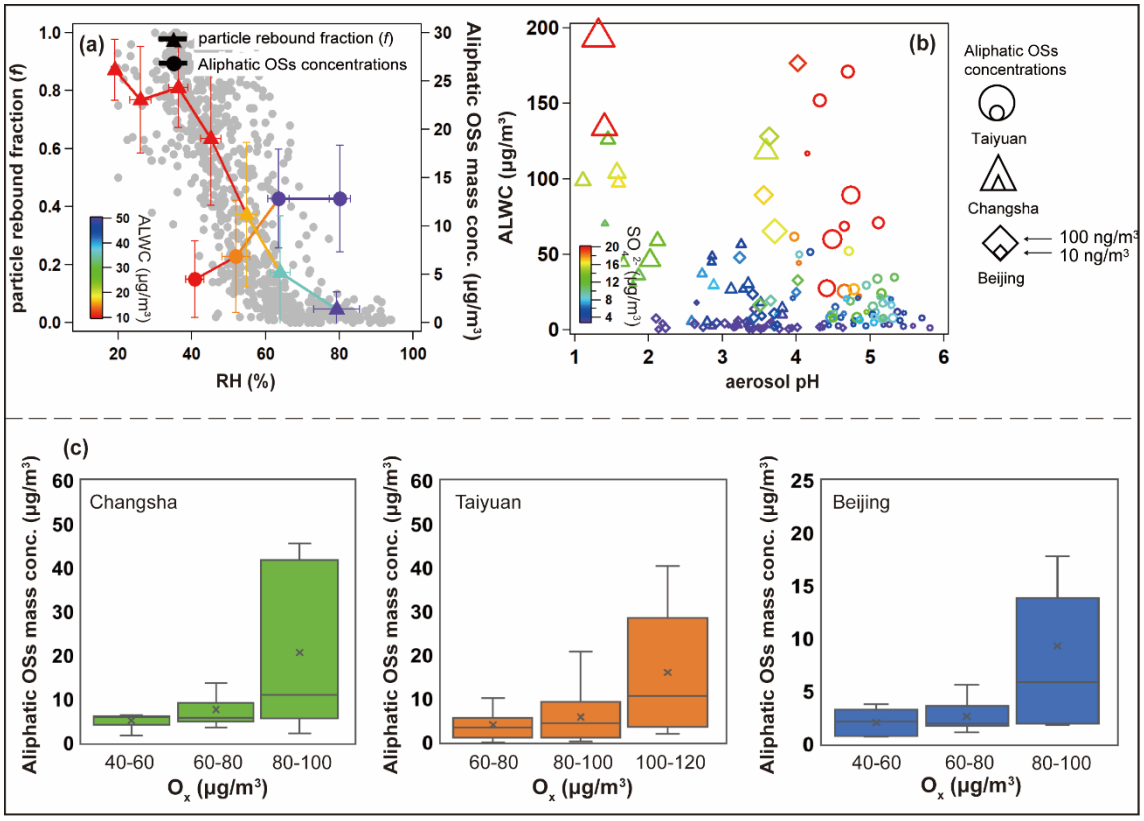

Figure 3 (a) The measured particle rebound fraction (*f*) and total mass concentrations of Aliphatic OSs ~~and NOSs~~ as a function of RH, the plots were colored by the calculated ALWC concentrations in Taiyuan, grey dots indicate the mass concentrations of Aliphatic OSs; (b) the relationship between aerosol pH and ALWC across three cities, the markers were colored by the inorganic sulfate mass concentrations, the marker sizes represented the total mass concentrations of Aliphatic OSs ~~and NOSs~~; (c) the box plot of total mass concentrations of Aliphatic OSs ~~and NOSs~~ at different O_x concentration levels.

This threshold behavior aligns with aerosol phase transitions. Particle rebound fraction (*f*), indicating phase state, was measured in Taiyuan using a three-arm impactor (Liu et al., 2017). As RH exceeded 60%, *f* dropped below 0.2 (Figure 3(a)), signaling a transition from non-liquid to liquid aerosol states. This transition at RH > 60% aligns with prior field (Liu et al., 2017; Liu et al., 2023; Meng et al., 2024; Song et al., 2022) and modeling (Qiu et al., 2023) studies in Eastern China.

Correspondingly, Aliphatic OSs concentrations increased with RH below 60% but plateaued beyond that despite further humidity rises. These findings underscore aerosol phase state as a critical factor: initial liquid phase formation (RH < 60%) promotes heterogeneous OS formation (Ye et al., 2018), whereas at higher RH, saturation of reactive interfaces limits further ALWC effects.

In addition, the increase in ALWC with rising RH altered aerosol pH (Figure 3(b)), which inhibited OSs formation via acid-catalyzed reactions (Duporté et al., 2016). In Changsha, as aerosol pH increased from ~~below~~ approximately 1.0 to above 3.0, the average total mass concentrations of Aliphatic OSs ~~and NOSs~~ decreased significantly from 9.3 to 4.6 ng/m^3 (Figure S8), with further declines as pH increased. In Taiyuan, OS concentrations dropped from 12.2 to 6.8 ng/m^3 as pH rose from below 4.5 to above 5.0. However, in Beijing, total mass concentrations of Aliphatic OSs ~~and NOSs~~ remained stable within a narrow pH range of 3.2–3.9. Elevated ALWC facilitates aqueous-phase radical chemistry that forms OSs via non-acid pathways, which can dominate over pH-dependent processes (Rudziński et al., 2009; Wach et al., 2019; Huang et al., 2019). Thus, pH-dependent suppression of Aliphatic OSs formation is common across urban aerosol pH ranges, but less evident when pH varies narrowly.

Inorganic sulfate plays a crucial role in OSs formation via sulfate esterification reactions (Xu et al., 2024; Wang et al., 2020). We thus examined its effect on the formation of Aliphatic OSs ~~and NOSs~~. Figure 3(b) illustrates the relationships among ALWC, pH, inorganic sulfate mass concentration, and total mass concentrations of Aliphatic OSs ~~and NOSs~~ across all cities. A consistent positive correlation was observed, consistent with previous field studies (Lin et al., 2022; Wang et al., 2023b; Le Breton et al., 2018; Wang et al., 2018). This correlation was strongest when sulfate concentrations were below 20 μg/m^3. Below this threshold, total mass concentrations of Aliphatic OSs ~~and NOSs~~ increased significantly with inorganic sulfate, whereas above it, the correlation weakened. Additionally, inorganic sulfate mass concentration showed a clear positive correlation with ALWC (Figure 3(b)), suggesting that ionic strength did not increase linearly with sulfate mass. This likely reflects saturation effects in acid-mediated pathways, driven by limitations in water activity and ionic strength (Wang et al., 2020). Overall, these results highlight the nonlinear influence of inorganic sulfate on Aliphatic OSs ~~and NOSs~~ formation.

Atmospheric oxidative capacity, represented by O_x ($O_x = O_3 + NO_2$) concentrations, typically modulates OS~~s~~ formation via acid-catalyzed ring-opening reactions pathways. As shown in Figure 3(c), total mass concentrations of Aliphatic OSs and NOSs exhibited significant increases with rising O_x levels across all cities. Especially, total mass concentrations of Aliphatic OSs ~~and NOSs~~ significantly increased across all cities when O_x concentrations raised from 60–80 μg/m^3 to > 80 μg/m^3. As shown in Figure S9, O_3 dominated the O_x composition during high-O_x episodes (> 80 μg/m^3) across all cities. Previous laboratory studies have suggested that enhanced atmospheric oxidation capacities promote ~~. Therefore, we inferred that high O_x conditions enhance~~ the oxidation of VOCs (Zhang et al., 2022; Wei et al., 2024), forming cyclic intermediates. We therefore inferred that the increase in O_x facilitates the formation of cyclic intermediates derived from long-chain alkenes. Subsequent acid-catalyzed and ring-opening reactions are important pathways of ~~leading to~~ heterogeneous OSs formation, including ~~–~~Aliphatic OSs ~~and NOSs formation via acid-catalyzed ring-opening reactions pathways~~ (Eddingsaas et al., 2010; Iinuma et al., 2007; Brüggemann et al., 2020).

4 Conclusions and Implications

In this study, we applied a NTA approach based on UHPLC-HRMS to investigate the molecular composition of OS~~s~~ in $PM_{2.5}$ samples from three cities. By integrating molecular composition data, precursor-constrained PMF source apportionment, and OS–precursor correlation analysis, we developed a comprehensive method for accurate classification of detected OSs, demonstrating superior discrimination between Aliphatic OSs ~~and NOSs~~. Conventional classification methods rely on laboratory chamber-derived precursor–OS relationships (Wang et al., 2019a), which provide limited insight into the formation of Aliphatic OSs ~~and NOSs~~ and tend to underestimate their mass fractions. The abundant Aliphatic OSs ~~and NOSs~~ detected in ambient $PM_{2.5}$ suggest complex formation pathways, such as OH oxidation of long-chain alkenes (Riva et al., 2016b) and heterogeneous SO_2–alkene reactions in acidic environments (Passananti et al., 2016), which remain incompletely understood in laboratory studies. Our findings highlight the importance of emphasizing the formation of Aliphatic OSs ~~and NOSs~~ in urban atmospheres.

However, this study still faces several challenges. This work was conducted during the winter. OS formation exhibits seasonal variability, particularly for pathways driven by biogenic VOCs emissions and photochemical activity, which are generally enhanced in warmer months. Hence, the underestimation of Aliphatic OSs, and their key formation factors determined in this work remain valid insights for the winter period but may not fully represent annual OS behavior. Future long-term observations are necessary to resolve the complete annual cycle of OS composition, quantify the shifting contributions of anthropogenic versus biogenic precursors, and understanding how key formation driving factors evolve with changing atmospheric conditions.

For NTA, the use of surrogate standards for quantification OS mass concentration introduced uncertainty, particularly due to the extraction efficiency of individual OSs species from quartz fiber filters could not be determined. Although we have adopted standardized extraction protocol ensures high comparability across our samples, absolute extraction recoveries may vary. In addition, this approach depends on public molecular composition such as mzCloud and ChemSpider integrated within the Compound Discoverer software, which contain limited entries for organosulfates. Reliance on these databases for compound identification may therefore underestimate OS mass concentrations in urban environments. ~~However, this approach depends on public molecular composition datasets, potentially underestimating OSs mass concentrations in urban environments.~~ For example, OSs identified here accounted for less than 1% of total OA mass, whereas recent work (Ma et al., 2025) reported approximately 20% contributions~~–~~.

~~Furthermore,~~ OS~~s~~ may become increasingly significant in OA, particularly in coastal regions influenced by oceanic dimethyl sulfate emissions (Brüggemann et al., 2020). Our ~~Future~~ future work will focus on synthesizing OSs standards representing various precursors and establishing a dedicated fragmentation database through multi-platform MS^2 validation to elucidate OS~~s~~ sources in more detail.

Author Contributions

Y.Q., J.W., and Z.W. designed this work. J.L., Y.Wei, C.L., J.Y., T.L., R.M., T.Z., W.F., J.Y., Z.F., Y.X. and K.B. collected $PM_{2.5}$ samples. Y.Q., J.W., T.Q., Y.B., and D.L. conducted UHPLC-HRMS

experiments. Y.Q., J.W., Z.G., and Y.Wang wrote this manuscript. Z.W., Y.Wang, and M.H. edited this manuscript. All authors have read and agreed to submit this manuscript. Y.Q. and J.W. contributed equally to this work.

Funding

This work is funded by the National Nature Science Foundation of China (Grants 22221004 and 22306059), This work was also supported by the Science and Technology Innovation Program of Hunan Province (Grants 2024RC3106 and 2025AQ2001), and the Fundamental Research Funds for the Central Universities (Grant 531118010830).

Notes

The authors declare that they have no conflict of interest.

Acknowledgements

Y.W would like to acknowledge financial support by the National Nature Science Foundation of China (Grants 22221004 and 22306059), This work was also supported by the Science and Technology Innovation Program of Hunan Province (Grants 2024RC3106 and 2025AQ2001), and the Fundamental Research Funds for the Central Universities (Grant 531118010830).

References

Bateman, A. P., Belassein, H., Martin, S. T.: Impactor Apparatus for the Study of Particle Rebound: Relative Humidity and Capillary Forces. Aerosol Science and Technology. 48, 42-52. 10.1080/02786826.2013.853866, 2014.

Brown, S. S., Dubé, W. P., Karamchandani, P., Yarwood, G., Peischl, J., Ryerson, T. B., Neuman, J. A., Nowak, J. B., Holloway, J. S., Washenfelder, R. A., Brock, C. A., Frost, G. J., Trainer, M., Parrish, D. D., Fehsenfeld, F. C., Ravishankara, A. R.: Effects of NOx control and plume mixing on nighttime chemical processing of plumes from coal-fired power plants. Journal of Geophysical Research: Atmospheres. 117. https://doi.org/10.1029/2011JD016954, 2012.

Brüggemann, M., Xu, R., Tilgner, A., Kwong, K. C., Mutzel, A., Poon, H. Y., Otto, T., Schaefer, T., Poulain, L., Chan, M. N., Herrmann, H.: Organosulfates in Ambient Aerosol: State of Knowledge and Future Research Directions on Formation, Abundance, Fate, and Importance. Environmental Science & Technology. 54, 3767-3782. 10.1021/acs.est.9b06751, 2020.

Cai, D., Wang, X., Chen, J., Li, X.: Molecular Characterization of Organosulfates in Highly Polluted Atmosphere Using Ultra-High-Resolution Mass Spectrometry. Journal of Geophysical Research: Atmospheres. 125, e2019JD032253. https://doi.org/10.1029/2019JD032253, 2020.

Cao, G., Zhao, X., Hu, D., Zhu, R., Ouyang, F.: Development and application of a quantification method for water soluble organosulfates in atmospheric aerosols. Environmental Pollution. 225, 316-322. https://doi.org/10.1016/j.envpol.2017.01.086, 2017.

Cheng, Y., Zheng, G., Wei, C., Mu, Q., Zheng, B., Wang, Z., Gao, M., Zhang, Q., He, K., Carmichael, G., Pöschl, U., Su, H.: Reactive nitrogen chemistry in aerosol water as a source of sulfate during haze events in China. Science Advances. 2, e1601530. 10.1126/sciadv.1601530, 2016a.

Cheng, Y., Zheng, G., Wei, C., Mu, Q., Zheng, B., Wang, Z., Gao, M., Zhang, Q., He, K., Carmichael, G., Pöschl, U., Su, H.: Reactive nitrogen chemistry in aerosol water as a source of sulfate during haze events in China. 2, e1601530. doi:10.1126/sciadv.1601530, 2016b.

Deng, Y., Inomata, S., Sato, K., Ramasamy, S., Morino, Y., Enami, S., Tanimoto, H.: Temperature and acidity dependence of secondary organic aerosol formation from α-pinene ozonolysis with a compact chamber system. Atmos. Chem. Phys. 21, 5983-6003. 10.5194/acp-21-5983-2021, 2021.

Ding, X., He, Q.-F., Shen, R.-Q., Yu, Q.-Q., Zhang, Y.-Q., Xin, J.-Y., Wen, T.-X., Wang, X.-M.: Spatial and seasonal variations of isoprene secondary organic aerosol in China: Significant impact of biomass burning during winter. Scientific Reports. 6, 20411. 10.1038/srep20411, 2016a.

Ding, X., Zhang, Y.-Q., He, Q.-F., Yu, Q.-Q., Shen, R.-Q., Zhang, Y., Zhang, Z., Lyu, S.-J., Hu, Q.-H., Wang, Y.-S., Li, L.-F., Song, W., Wang, X.-M.: Spatial and seasonal variations of secondary organic aerosol from terpenoids over China. Journal of Geophysical Research: Atmospheres. 121, 14,661-614,678. https://doi.org/10.1002/2016JD025467, 2016b.

Duporté, G., Flaud, P. M., Geneste, E., Augagneur, S., Pangui, E., Lamkaddam, H., Gratien, A., Doussin, J. F., Budzinski, H., Villenave, E., Perraudin, E.: Experimental Study of the Formation of

Organosulfates from α-Pinene Oxidation. Part I: Product Identification, Formation Mechanisms and Effect of Relative Humidity. The Journal of Physical Chemistry A. 120, 7909-7923. 10.1021/acs.jpca.6b08504, 2016.

Duporté, G., Flaud, P. M., Kammer, J., Geneste, E., Augagneur, S., Pangui, E., Lamkaddam, H., Gratien, A., Doussin, J. F., Budzinski, H., Villenave, E., Perraudin, E.: Experimental Study of the Formation of Organosulfates from α-Pinene Oxidation. 2. Time Evolution and Effect of Particle Acidity. The Journal of Physical Chemistry A. 124, 409-421. 10.1021/acs.jpca.9b07156, 2020.

Eddingsaas, N. C., VanderVelde, D. G., Wennberg, P. O.: Kinetics and Products of the Acid-Catalyzed Ring-Opening of Atmospherically Relevant Butyl Epoxy Alcohols. The Journal of Physical Chemistry A. 114, 8106-8113. 10.1021/jp103907c, 2010.

Edwards, P. M., Aikin, K. C., Dube, W. P., Fry, J. L., Gilman, J. B., de Gouw, J. A., Graus, M. G., Hanisco, T. F., Holloway, J., Hübler, G., Kaiser, J., Keutsch, F. N., Lerner, B. M., Neuman, J. A., Parrish, D. D., Peischl, J., Pollack, I. B., Ravishankara, A. R., Roberts, J. M., Ryerson, T. B., Trainer, M., Veres, P. R., Wolfe, G. M., Warneke, C., Brown, S. S.: Transition from high- to low-NOx control of night-time oxidation in the southeastern US. Nature Geoscience. 10, 490-495. 10.1038/ngeo2976, 2017.

Estillore, A. D., Hettiyadura, A. P. S., Qin, Z., Leckrone, E., Wombacher, B., Humphry, T., Stone, E. A., Grassian, V. H.: Water Uptake and Hygroscopic Growth of Organosulfate Aerosol. Environmental Science & Technology. 50, 4259-4268. 10.1021/acs.est.5b05014, 2016.

Fleming, L. T., Ali, N. N., Blair, S. L., Roveretto, M., George, C., Nizkorodov, S. A.: Formation of Light-Absorbing Organosulfates during Evaporation of Secondary Organic Material Extracts in the Presence of Sulfuric Acid. ACS Earth and Space Chemistry. 3, 947-957. 10.1021/acsearthspacechem.9b00036, 2019.

Fountoukis, C., Nenes, A.: ISORROPIA II: a computationally efficient thermodynamic equilibrium model for K+; Ca2+; Mg2+; NH4+; Na+; SO42-; NO3-; Cl-; H2O aerosols. Atmospheric Chemistry and Physics. 7, 4639-4659. 10.5194/acp-7-4639-2007, 2007.

Guenther, A., Karl, T., Harley, P., Wiedinmyer, C., Palmer, P. I., Geron, C.: Estimates of global terrestrial isoprene emissions using MEGAN (Model of Emissions of Gases and Aerosols from Nature). Atmos. Chem. Phys. 6, 3181-3210. 10.5194/acp-6-3181-2006, 2006.

Hansen, A. M. K., Hong, J., Raatikainen, T., Kristensen, K., Ylisirniö, A., Virtanen, A., Petäjä, T., Glasius, M., Prisle, N. L.: Hygroscopic properties and cloud condensation nuclei activation of limonene-derived organosulfates and their mixtures with ammonium sulfate. Atmos. Chem. Phys. 15, 14071-14089. 10.5194/acp-15-14071-2015, 2015.

He, J., Li, L., Li, Y., Huang, M., Zhu, Y., Deng, S.: Synthesis, MS/MS characteristics and quantification of six aromatic organosulfates in atmospheric PM2.5. Atmospheric Environment. 290, 119361. https://doi.org/10.1016/j.atmosenv.2022.119361, 2022.

Hettiyadura, A. P. S., Jayarathne, T., Baumann, K., Goldstein, A. H., de Gouw, J. A., Koss, A., Keutsch, F. N., Skog, K., Stone, E. A.: Qualitative and quantitative analysis of atmospheric organosulfates in Centreville, Alabama. Atmospheric Chemistry and Physics. 17, 1343-1359. 10.5194/acp-17-1343-2017, 2017.

572 Hoyle, C. R., Boy, M., Donahue, N. M., Fry, J. L., Glasius, M., Guenther, A., Hallar, A. G., Huff Hartz,
573 K., Petters, M. D., Petäjä, T., Rosenoern, T., Sullivan, A. P.: A review of the anthropogenic influence on
574 biogenic secondary organic aerosol. Atmos. Chem. Phys. 11, 321-343. 10.5194/acp-11-321-2011, 2011.

575 Huang, L., Cochran, R. E., Coddens, E. M., Grassian, V. H.: Formation of Organosulfur Compounds
576 through Transition Metal Ion-Catalyzed Aqueous Phase Reactions. Environmental Science & Technology
577 Letters. 5, 315-321. 10.1021/acs.estlett.8b00225, 2018a.

578 Huang, L., Coddens, E. M., Grassian, V. H.: Formation of Organosulfur Compounds from Aqueous
579 Phase Reactions of S(IV) with Methacrolein and Methyl Vinyl Ketone in the Presence of Transition Metal
580 Ions. ACS Earth and Space Chemistry. 3, 1749-1755. 10.1021/acsearthspacechem.9b00173, 2019.

581 Huang, L., Liu, T., Grassian, V. H.: Radical-Initiated Formation of Aromatic Organosulfates and
582 Sulfonates in the Aqueous Phase. Environmental Science & Technology. 54, 11857-11864.
583 10.1021/acs.est.0c05644, 2020.

584 Huang, L., Wang, Y., Zhao, Y., Hu, H., Yang, Y., Wang, Y., Yu, J.-Z., Chen, T., Cheng, Z., Li, C., Li,
585 Z., Xiao, H.: Biogenic and Anthropogenic Contributions to Atmospheric Organosulfates in a Typical
586 Megacity in Eastern China. Journal of Geophysical Research: Atmospheres. 128, e2023JD038848.
587 https://doi.org/10.1029/2023JD038848, 2023a.

588 Huang, L., Wang, Y., Zhao, Y., Hu, H., Yang, Y., Wang, Y., Yu, J.-Z., Chen, T., Cheng, Z., Li, C., Li,
589 Z., Xiao, H.: Biogenic and Anthropogenic Contributions to Atmospheric Organosulfates in a Typical
590 Megacity in Eastern China. 128, e2023JD038848. https://doi.org/10.1029/2023JD038848, 2023b.

591 Huang, R. J., Cao, J., Chen, Y., Yang, L., Shen, J., You, Q., Wang, K., Lin, C., Xu, W., Gao, B., Li, Y.,
592 Chen, Q., Hoffmann, T., O'Dowd, C. D., Bilde, M., Glasius, M.: Organosulfates in atmospheric aerosol:
593 synthesis and quantitative analysis of PM2.5 from Xi'an, northwestern China. Atmos. Meas. Tech. 11, 3447-
594 3456. 10.5194/amt-11-3447-2018, 2018b.

595 Iinuma, Y., Müller, C., Berndt, T., Böge, O., Claeys, M., Herrmann, H.: Evidence for the Existence of
596 Organosulfates from β-Pinene Ozonolysis in Ambient Secondary Organic Aerosol. Environmental Science
597 & Technology. 41, 6678-6683. 10.1021/es070938t, 2007.

598 Jiang, H., Cai, J., Feng, X., Chen, Y., Guo, H., Mo, Y., Tang, J., Chen, T., Li, J., Zhang, G.:
599 Organosulfur Compounds: A Non-Negligible Component Affecting the Light Absorption of Brown Carbon
600 During North China Haze Events. Journal of Geophysical Research: Atmospheres. 130, e2024JD042043.
601 https://doi.org/10.1029/2024JD042043, 2025.

602 Koss, A. R., Sekimoto, K., Gilman, J. B., Selimovic, V., Coggon, M. M., Zarzana, K. J., Yuan, B.,
603 Lerner, B. M., Brown, S. S., Jimenez, J. L., Krechmer, J., Roberts, J. M., Warneke, C., Yokelson, R. J., de
604 Gouw, J.: Non-methane organic gas emissions from biomass burning: identification, quantification, and
605 emission factors from PTR-ToF during the FIREX 2016 laboratory experiment. Atmos. Chem. Phys. 18,
606 3299-3319. 10.5194/acp-18-3299-2018, 2018.

607 Le Breton, M., Wang, Y., Hallquist, Å. M., Pathak, R. K., Zheng, J., Yang, Y., Shang, D., Glasius, M.,
608 Bannan, T. J., Liu, Q., Chan, C. K., Percival, C. J., Zhu, W., Lou, S., Topping, D., Wang, Y., Yu, J., Lu, K.,
609 Guo, S., Hu, M., Hallquist, M.: Online gas- and particle-phase measurements of organosulfates,
610 organosulfonates and nitrooxy organosulfates in Beijing utilizing a FIGAERO ToF-CIMS. Atmos. Chem.

Phys. 18, 10355-10371. 10.5194/acp-18-10355-2018, 2018.

Li, L., Yang, W., Xie, S., Wu, Y.: Estimations and uncertainty of biogenic volatile organic compound emission inventory in China for 2008–2018. Science of The Total Environment. 733, 139301. https://doi.org/10.1016/j.scitotenv.2020.139301, 2020.

Lin, P., Yu, J. Z., Engling, G., Kalberer, M.: Organosulfates in Humic-like Substance Fraction Isolated from Aerosols at Seven Locations in East Asia: A Study by Ultra-High-Resolution Mass Spectrometry. Environmental Science & Technology. 46, 13118-13127. 10.1021/es303570v, 2012.

Lin, Y., Han, Y., Li, G., Wang, Q., Zhang, X., Li, Z., Li, L., Prévôt, A. S. H., Cao, J.: Molecular Characteristics of Atmospheric Organosulfates During Summer and Winter Seasons in Two Cities of Southern and Northern China. Journal of Geophysical Research: Atmospheres. 127, e2022JD036672. https://doi.org/10.1029/2022JD036672, 2022.

Liu, P., Ding, X., Li, B. X., Zhang, Y. Q., Bryant, D. J., Wang, X. M.: Quality assurance and quality control of atmospheric organosulfates measured using hydrophilic interaction liquid chromatography (HILIC). Atmos. Meas. Tech. 17, 3067-3079. 10.5194/amt-17-3067-2024, 2024.

Liu, Y., Wu, Z., Wang, Y., Xiao, Y., Gu, F., Zheng, J., Tan, T., Shang, D., Wu, Y., Zeng, L., Hu, M., Bateman, A. P., Martin, S. T.: Submicrometer Particles Are in the Liquid State during Heavy Haze Episodes in the Urban Atmosphere of Beijing, China. Environ. Sci. Technol. Lett. 4, 427-432. 10.1021/acs.estlett.7b00352, 2017.

Liu, Y. C., Wu, Z. J., Qiu, Y. T., Tian, P., Liu, Q., Chen, Y., Song, M., Hu, M.: Enhanced Nitrate Fraction: Enabling Urban Aerosol Particles to Remain in a Liquid State at Reduced Relative Humidity. Geophysical Research Letters. 50, e2023GL105505. https://doi.org/10.1029/2023GL105505, 2023.

Lukács, H., Gelencsér, A., Hoffer, A., Kiss, G., Horváth, K., Hartyáni, Z.: Quantitative assessment of organosulfates in size-segregated rural fine aerosol. Atmos. Chem. Phys. 9, 231-238. 10.5194/acp-9-231-2009, 2009.

Ma, J., Ungeheuer, F., Zheng, F., Du, W., Wang, Y., Cai, J., Zhou, Y., Yan, C., Liu, Y., Kulmala, M., Daellenbach, K. R., Vogel, A. L.: Nontarget Screening Exhibits a Seasonal Cycle of PM2.5 Organic Aerosol Composition in Beijing. Environmental Science & Technology. 56, 7017-7028. 10.1021/acs.est.1c06905, 2022.

Ma, J., Reininger, N., Zhao, C., Döbler, D., Rüdiger, J., Qiu, Y., Ungeheuer, F., Simon, M., D'Angelo, L., Breuninger, A., David, J., Bai, Y., Li, Y., Xue, Y., Li, L., Wang, Y., Hildmann, S., Hoffmann, T., Liu, B., Niu, H., Wu, Z., Vogel, A. L.: Unveiling a large fraction of hidden organosulfates in ambient organic aerosol. Nature Communications. 16, 4098. 10.1038/s41467-025-59420-y, 2025.

Meng, X., Wu, Z., Chen, J., Qiu, Y., Zong, T., Song, M., Lee, J., Hu, M.: Particle phase state and aerosol liquid water greatly impact secondary aerosol formation: insights into phase transition and its role in haze events. Atmospheric Chemistry and Physics. 24, 2399-2414. 10.5194/acp-24-2399-2024, 2024.

Mutzel, A., Poulain, L., Berndt, T., Iinuma, Y., Rodigast, M., Böge, O., Richters, S., Spindler, G., Sipilä, M., Jokinen, T., Kulmala, M., Herrmann, H.: Highly Oxidized Multifunctional Organic Compounds Observed in Tropospheric Particles: A Field and Laboratory Study. Environmental Science & Technology.

49, 7754-7761. 10.1021/acs.est.5b00885, 2015.

Ohno, P. E., Wang, J., Mahrt, F., Varelas, J. G., Aruffo, E., Ye, J., Qin, Y., Kiland, K. J., Bertram, A. K., Thomson, R. J., Martin, S. T.: Gas-Particle Uptake and Hygroscopic Growth by Organosulfate Particles. ACS Earth and Space Chemistry. 6, 2481-2490. 10.1021/acsearthspacechem.2c00195, 2022.

Passananti, M., Kong, L., Shang, J., Dupart, Y., Perrier, S., Chen, J., Donaldson, D. J., George, C.: Organosulfate Formation through the Heterogeneous Reaction of Sulfur Dioxide with Unsaturated Fatty Acids and Long-Chain Alkenes. Angewandte Chemie International Edition. 55, 10336-10339. https://doi.org/10.1002/anie.201605266, 2016.

Qiu, Y., Liu, Y., Wu, Z., Wang, F., Meng, X., Zhang, Z., Man, R., Huang, D., Wang, H., Gao, Y., Huang, C., Hu, M.: Predicting Atmospheric Particle Phase State Using an Explainable Machine Learning Approach Based on Particle Rebound Measurements. Environmental Science & Technology. 57, 15055-15064. 10.1021/acs.est.3c05284, 2023.

Riva, M., Tomaz, S., Cui, T., Lin, Y.-H., Perraudin, E., Gold, A., Stone, E. A., Villenave, E., Surratt, J. D.: Evidence for an Unrecognized Secondary Anthropogenic Source of Organosulfates and Sulfonates: Gas-Phase Oxidation of Polycyclic Aromatic Hydrocarbons in the Presence of Sulfate Aerosol. Environmental Science & Technology. 49, 6654-6664. 10.1021/acs.est.5b00836, 2015.

Riva, M., Budisulistiorini, S. H., Zhang, Z., Gold, A., Surratt, J. D.: Chemical characterization of secondary organic aerosol constituents from isoprene ozonolysis in the presence of acidic aerosol. Atmospheric Environment. 130, 5-13. https://doi.org/10.1016/j.atmosenv.2015.06.027, 2016a.

Riva, M., Da Silva Barbosa, T., Lin, Y. H., Stone, E. A., Gold, A., Surratt, J. D.: Chemical characterization of organosulfates in secondary organic aerosol derived from the photooxidation of alkanes. Atmospheric Chemistry and Physics. 16, 11001-11018. 10.5194/acp-16-11001-2016, 2016b.

Riva, M., Da Silva Barbosa, T., Lin, Y. H., Stone, E. A., Gold, A., Surratt, J. D.: Chemical characterization of organosulfates in secondary organic aerosol derived from the photooxidation of alkanes. Atmos. Chem. Phys. 16, 11001-11018. 10.5194/acp-16-11001-2016, 2016c.

Riva, M., Chen, Y., Zhang, Y., Lei, Z., Olson, N. E., Boyer, H. C., Narayan, S., Yee, L. D., Green, H. S., Cui, T., Zhang, Z., Baumann, K., Fort, M., Edgerton, E., Budisulistiorini, S. H., Rose, C. A., Ribeiro, I. O., e Oliveira, R. L., dos Santos, E. O., Machado, C. M. D., Szopa, S., Zhao, Y., Alves, E. G., de Sá, S. S., Hu, W., Knipping, E. M., Shaw, S. L., Duvoisin Junior, S., de Souza, R. A. F., Palm, B. B., Jimenez, J.-L., Glasius, M., Goldstein, A. H., Pye, H. O. T., Gold, A., Turpin, B. J., Vizuete, W., Martin, S. T., Thornton, J. A., Dutcher, C. S., Ault, A. P., Surratt, J. D.: Increasing Isoprene Epoxydiol-to-Inorganic Sulfate Aerosol Ratio Results in Extensive Conversion of Inorganic Sulfate to Organosulfur Forms: Implications for Aerosol Physicochemical Properties. Environmental Science & Technology. 53, 8682-8694. 10.1021/acs.est.9b01019, 2019.

Rudziński, K. J., Gmachowski, L., Kuznietsova, I.: Reactions of isoprene and sulphoxy radical-anions – a possible source of atmospheric organosulphites and organosulphates. Atmos. Chem. Phys. 9, 2129-2140. 10.5194/acp-9-2129-2009, 2009.

Sakulyanontvittaya, T., Guenther, A., Helmig, D., Milford, J., Wiedinmyer, C.: Secondary Organic Aerosol from Sesquiterpene and Monoterpene Emissions in the United States. Environmental Science &

688 Technology. 42, 8784-8790. 10.1021/es800817r, 2008.

689 Song, M., Jeong, R., Kim, D., Qiu, Y., Meng, X., Wu, Z., Zuend, A., Ha, Y., Kim, C., Kim, H., Gaikwad,
690 S., Jang, K. S., Lee, J. Y., Ahn, J.: Comparison of Phase States of PM2.5over Megacities, Seoul and Beijing,
691 and Their Implications on Particle Size Distribution. Environmental Science and Technology. 56, 17581-
692 17590. 10.1021/acs.est.2c06377, 2022.

693 Staudt, S., Kundu, S., Lehmler, H.-J., He, X., Cui, T., Lin, Y.-H., Kristensen, K., Glasius, M., Zhang,
694 X., Weber, R. J., Surratt, J. D., Stone, E. A.: Aromatic organosulfates in atmospheric aerosols: Synthesis,
695 characterization, and abundance. Atmospheric Environment. 94, 366-373.
696 https://doi.org/10.1016/j.atmosenv.2014.05.049, 2014.

697 Surratt, J. D., Gómez-González, Y., Chan, A. W. H., Vermeylen, R., Shahgholi, M., Kleindienst, T. E.,
698 Edney, E. O., Offenberg, J. H., Lewandowski, M., Jaoui, M., Maenhaut, W., Claeys, M., Flagan, R. C.,
699 Seinfeld, J. H.: Organosulfate Formation in Biogenic Secondary Organic Aerosol. The Journal of Physical
700 Chemistry A. 112, 8345-8378. 10.1021/jp802310p, 2008.

701 Tang, J., Li, J., Su, T., Han, Y., Mo, Y., Jiang, H., Cui, M., Jiang, B., Chen, Y., Tang, J., Song, J., Peng,
702 P., Zhang, G.: Molecular compositions and optical properties of dissolved brown carbon in biomass burning,
703 coal combustion, and vehicle emission aerosols illuminated by excitation–emission matrix spectroscopy
704 and Fourier transform ion cyclotron resonance mass spectrometry analysis. Atmos. Chem. Phys. 20, 2513-
705 2532. 10.5194/acp-20-2513-2020, 2020.

706 Tao, S., Lu, X., Levac, N., Bateman, A. P., Nguyen, T. B., Bones, D. L., Nizkorodov, S. A., Laskin, J.,
707 Laskin, A., Yang, X.: Molecular Characterization of Organosulfates in Organic Aerosols from Shanghai and
708 Los Angeles Urban Areas by Nanospray-Desorption Electrospray Ionization High-Resolution Mass
709 Spectrometry. Environmental Science & Technology. 48, 10993-11001. 10.1021/es5024674, 2014.

710 Tolocka, M. P., Turpin, B.: Contribution of Organosulfur Compounds to Organic Aerosol Mass.
711 Environmental Science & Technology. 46, 7978-7983. 10.1021/es300651v, 2012.

712 Wach, P., Spólnik, G., Rudziński, K. J., Skotak, K., Claeys, M., Danikiewicz, W., Szmigielski, R.:
713 Radical oxidation of methyl vinyl ketone and methacrolein in aqueous droplets: Characterization of
714 organosulfates and atmospheric implications. Chemosphere. 214, 1-9.
715 https://doi.org/10.1016/j.chemosphere.2018.09.026, 2019.

716 Wang, G., Zhang, R., Gomez, M. E., Yang, L., Levy Zamora, M., Hu, M., Lin, Y., Peng, J., Guo, S.,
717 Meng, J., Li, J., Cheng, C., Hu, T., Ren, Y., Wang, Y., Gao, J., Cao, J., An, Z., Zhou, W., Li, G., Wang, J.,
718 Tian, P., Marrero-Ortiz, W., Secrest, J., Du, Z., Zheng, J., Shang, D., Zeng, L., Shao, M., Wang, W., Huang,
719 Y., Wang, Y., Zhu, Y., Li, Y., Hu, J., Pan, B., Cai, L., Cheng, Y., Ji, Y., Zhang, F., Rosenfeld, D., Liss, P. S.,
720 Duce, R. A., Kolb, C. E., Molina, M. J.: Persistent sulfate formation from London Fog to Chinese haze.
721 Proceedings of the National Academy of Sciences. 113, 13630-13635. 10.1073/pnas.1616540113, 2016a.

722 Wang, G., Zhang, R., Gomez, M. E., Yang, L., Levy Zamora, M., Hu, M., Lin, Y., Peng, J., Guo, S.,
723 Meng, J., Li, J., Cheng, C., Hu, T., Ren, Y., Wang, Y., Gao, J., Cao, J., An, Z., Zhou, W., Li, G., Wang, J.,
724 Tian, P., Marrero-Ortiz, W., Secrest, J., Du, Z., Zheng, J., Shang, D., Zeng, L., Shao, M., Wang, W., Huang,
725 Y., Wang, Y., Zhu, Y., Li, Y., Hu, J., Pan, B., Cai, L., Cheng, Y., Ji, Y., Zhang, F., Rosenfeld, D., Liss, P. S.,
726 Duce, R. A., Kolb, C. E., Molina, M. J.: Persistent sulfate formation from London Fog to Chinese haze.

113, 13630-13635. doi:10.1073/pnas.1616540113, 2016b.

Wang, H., Ma, X., Tan, Z., Wang, H., Chen, X., Chen, S., Gao, Y., Liu, Y., Liu, Y., Yang, X., Yuan, B., Zeng, L., Huang, C., Lu, K., Zhang, Y.: Anthropogenic monoterpenes aggravating ozone pollution. National Science Review. 9, nwac103. 10.1093/nsr/nwac103, 2022a.

Wang, K., Zhang, Y., Huang, R.-J., Wang, M., Ni, H., Kampf, C. J., Cheng, Y., Bilde, M., Glasius, M., Hoffmann, T.: Molecular Characterization and Source Identification of Atmospheric Particulate Organosulfates Using Ultrahigh Resolution Mass Spectrometry. Environmental Science & Technology. 53, 6192-6202. 10.1021/acs.est.9b02628, 2019a.

Wang, Y., Ren, J., Huang, X. H. H., Tong, R., Yu, J. Z.: Synthesis of Four Monoterpene-Derived Organosulfates and Their Quantification in Atmospheric Aerosol Samples. Environmental Science & Technology. 51, 6791-6801. 10.1021/acs.est.7b01179, 2017.

Wang, Y., Hu, M., Guo, S., Wang, Y., Zheng, J., Yang, Y., Zhu, W., Tang, R., Li, X., Liu, Y., Le Breton, M., Du, Z., Shang, D., Wu, Y., Wu, Z., Song, Y., Lou, S., Hallquist, M., Yu, J.: The secondary formation of organosulfates under interactions between biogenic emissions and anthropogenic pollutants in summer in Beijing. Atmospheric Chemistry and Physics. 18, 10693-10713. 10.5194/acp-18-10693-2018, 2018.

Wang, Y., Ma, Y., Li, X., Kuang, B. Y., Huang, C., Tong, R., Yu, J. Z.: Monoterpene and Sesquiterpene α-Hydroxy Organosulfates: Synthesis, MS/MS Characteristics, and Ambient Presence. Environmental Science & Technology. 53, 12278-12290. 10.1021/acs.est.9b04703, 2019b.

Wang, Y., Hu, M., Wang, Y.-C., Li, X., Fang, X., Tang, R., Lu, S., Wu, Y., Guo, S., Wu, Z., Hallquist, M., Yu, J. Z.: Comparative Study of Particulate Organosulfates in Contrasting Atmospheric Environments: Field Evidence for the Significant Influence of Anthropogenic Sulfate and NOx. Environmental Science & Technology Letters. 7, 787-794. 10.1021/acs.estlett.0c00550, 2020.

Wang, Y., Zhao, Y., Wang, Y., Yu, J. Z., Shao, J., Liu, P., Zhu, W., Cheng, Z., Li, Z., Yan, N., Xiao, H.: Organosulfates in atmospheric aerosols in Shanghai, China: seasonal and interannual variability, origin, and formation mechanisms. Atmos. Chem. Phys. 21, 2959-2980. 10.5194/acp-21-2959-2021, 2021a.

Wang, Y., Zhao, Y., Wang, Y., Yu, J. Z., Shao, J., Liu, P., Zhu, W., Cheng, Z., Li, Z., Yan, N., Xiao, H.: Organosulfates in atmospheric aerosols in Shanghai, China: seasonal and interannual variability, origin, and formation mechanisms. Atmospheric Chemistry and Physics. 21, 2959-2980. 10.5194/acp-21-2959-2021, 2021b.

Wang, Y., Ma, Y., Kuang, B., Lin, P., Liang, Y., Huang, C., Yu, J. Z.: Abundance of organosulfates derived from biogenic volatile organic compounds: Seasonal and spatial contrasts at four sites in China. Science of The Total Environment. 806, 151275. https://doi.org/10.1016/j.scitotenv.2021.151275, 2022b.

Wang, Y., Feng, Z., Yuan, Q., Shang, D., Fang, Y., Guo, S., Wu, Z., Zhang, C., Gao, Y., Yao, X., Gao, H., Hu, M.: Environmental factors driving the formation of water-soluble organic aerosols: A comparative study under contrasting atmospheric conditions. Science of The Total Environment. 866, 161364. https://doi.org/10.1016/j.scitotenv.2022.161364, 2023a.

Wang, Y., Liang, S., Le Breton, M., Wang, Q. Q., Liu, Q., Ho, C. H., Kuang, B. Y., Wu, C., Hallquist, M., Tong, R., Yu, J. Z.: Field observations of C2 and C3 organosulfates and insights into their formation

765 mechanisms at a suburban site in Hong Kong. Science of The Total Environment. 904, 166851.
766 https://doi.org/10.1016/j.scitotenv.2023.166851, 2023b.

767 Wei, L., Liu, R., Liao, C., Ouyang, S., Wu, Y., Jiang, B., Chen, D., Zhang, T., Guo, Y., Liu, S. C.: An
768 observation-based analysis of atmospheric oxidation capacity in Guangdong, China. Atmospheric
769 Environment. 318, 120260. https://doi.org/10.1016/j.atmosenv.2023.120260, 2024.

770 Wu, Z., Wang, Y., Tan, T., Zhu, Y., Li, M., Shang, D., Wang, H., Lu, K., Guo, S., Zeng, L., Zhang, Y.:
771 Aerosol Liquid Water Driven by Anthropogenic Inorganic Salts: Implying Its Key Role in Haze Formation
772 over the North China Plain. Environmental Science & Technology Letters. 5, 160-166.
773 10.1021/acs.estlett.8b00021, 2018.

774 Xu, L., Tsona, N. T., Du, L.: Relative Humidity Changes the Role of SO2 in Biogenic Secondary
775 Organic Aerosol Formation. The Journal of Physical Chemistry Letters. 12, 7365-7372.
776 10.1021/acs.jpclett.1c01550, 2021a.

777 Xu, L., Yang, Z., Tsona, N. T., Wang, X., George, C., Du, L.: Anthropogenic–Biogenic Interactions at
778 Night: Enhanced Formation of Secondary Aerosols and Particulate Nitrogen- and Sulfur-Containing
779 Organics from β-Pinene Oxidation. Environmental Science & Technology. 55, 7794-7807.
780 10.1021/acs.est.0c07879, 2021b.

781 Xu, R., Chen, Y., Ng, S. I. M., Zhang, Z., Gold, A., Turpin, B. J., Ault, A. P., Surratt, J. D., Chan, M.
782 N.: Formation of Inorganic Sulfate and Volatile Nonsulfated Products from Heterogeneous Hydroxyl
783 Radical Oxidation of 2-Methyltetrol Sulfate Aerosols: Mechanisms and Atmospheric Implications.
784 Environmental Science & Technology Letters. 11, 968-974. 10.1021/acs.estlett.4c00451, 2024.

785 Yang, T., Xu, Y., Ye, Q., Ma, Y. J., Wang, Y. C., Yu, J. Z., Duan, Y. S., Li, C. X., Xiao, H. W., Li, Z. Y.,
786 Zhao, Y., Xiao, H. Y.: Spatial and diurnal variations of aerosol organosulfates in summertime Shanghai,
787 China: potential influence of photochemical processes and anthropogenic sulfate pollution. Atmos. Chem.
788 Phys. 23, 13433-13450. 10.5194/acp-23-13433-2023, 2023.

789 Yang, T., Xu, Y., Ma, Y.-J., Wang, Y.-C., Yu, J. Z., Sun, Q.-B., Xiao, H.-W., Xiao, H.-Y., Liu, C.-Q.:
790 Field Evidence for Constraints of Nearly Dry and Weakly Acidic Aerosol Conditions on the Formation of
791 Organosulfates. Environmental Science & Technology Letters. 11, 981-987. 10.1021/acs.estlett.4c00522,
792 2024.

793 Yassine, M. M., Harir, M., Dabek-Zlotorzynska, E., Schmitt-Kopplin, P.: Structural characterization
794 of organic aerosol using Fourier transform ion cyclotron resonance mass spectrometry: Aromaticity
795 equivalent approach. Rapid Communications in Mass Spectrometry. 28, 2445-2454.
796 https://doi.org/10.1002/rcm.7038, 2014.

797 Ye, C., Lu, K., Song, H., Mu, Y., Chen, J., Zhang, Y.: A critical review of sulfate aerosol formation
798 mechanisms during winter polluted periods. Journal of Environmental Sciences. 123, 387-399.
799 https://doi.org/10.1016/j.jes.2022.07.011, 2023.

800 Ye, J., Abbatt, J. P. D., Chan, A. W. H.: Novel pathway of SO2 oxidation in the atmosphere: reactions
801 with monoterpene ozonolysis intermediates and secondary organic aerosol. Atmos. Chem. Phys. 18, 5549-
802 5565. 10.5194/acp-18-5549-2018, 2018.

Zhang, Y., Chen, Y., Lei, Z., Olson, N. E., Riva, M., Koss, A. R., Zhang, Z., Gold, A., Jayne, J. T., Worsnop, D. R., Onasch, T. B., Kroll, J. H., Turpin, B. J., Ault, A. P., Surratt, J. D.: Joint Impacts of Acidity and Viscosity on the Formation of Secondary Organic Aerosol from Isoprene Epoxydiols (IEPOX) in Phase Separated Particles. ACS Earth and Space Chemistry. 3, 2646-2658. 10.1021/acsearthspacechem.9b00209, 2019.

Zhang, Z., Jiang, J., Lu, B., Meng, X., Herrmann, H., Chen, J., Li, X.: Attributing Increases in Ozone to Accelerated Oxidation of Volatile Organic Compounds at Reduced Nitrogen Oxides Concentrations. PNAS Nexus. 1, pgac266. 10.1093/pnasnexus/pgac266, 2022.

Zhao, D., Schmitt, S. H., Wang, M., Acir, I. H., Tillmann, R., Tan, Z., Novelli, A., Fuchs, H., Pullinen, I., Wegener, R., Rohrer, F., Wildt, J., Kiendler-Scharr, A., Wahner, A., Mentel, T. F.: Effects of NOx and SO2 on the secondary organic aerosol formation from photooxidation of α-pinene and limonene. Atmos. Chem. Phys. 18, 1611-1628. 10.5194/acp-18-1611-2018, 2018.

Zheng, B., Zhang, Q., Zhang, Y., He, K. B., Wang, K., Zheng, G. J., Duan, F. K., Ma, Y. L., Kimoto, T.: Heterogeneous chemistry: a mechanism missing in current models to explain secondary inorganic aerosol formation during the January 2013 haze episode in North China. Atmos. Chem. Phys. 15, 2031-2049. 10.5194/acp-15-2031-2015, 2015.